Smart Materials

DOI: 10.1002/anie.201400370

Self-assembled Dynamic 3D Fingerprints in Liquid-Crystal Coatings Towards Controllable Friction and Adhesion**

*Danqing Liu and Dirk J. Broer**

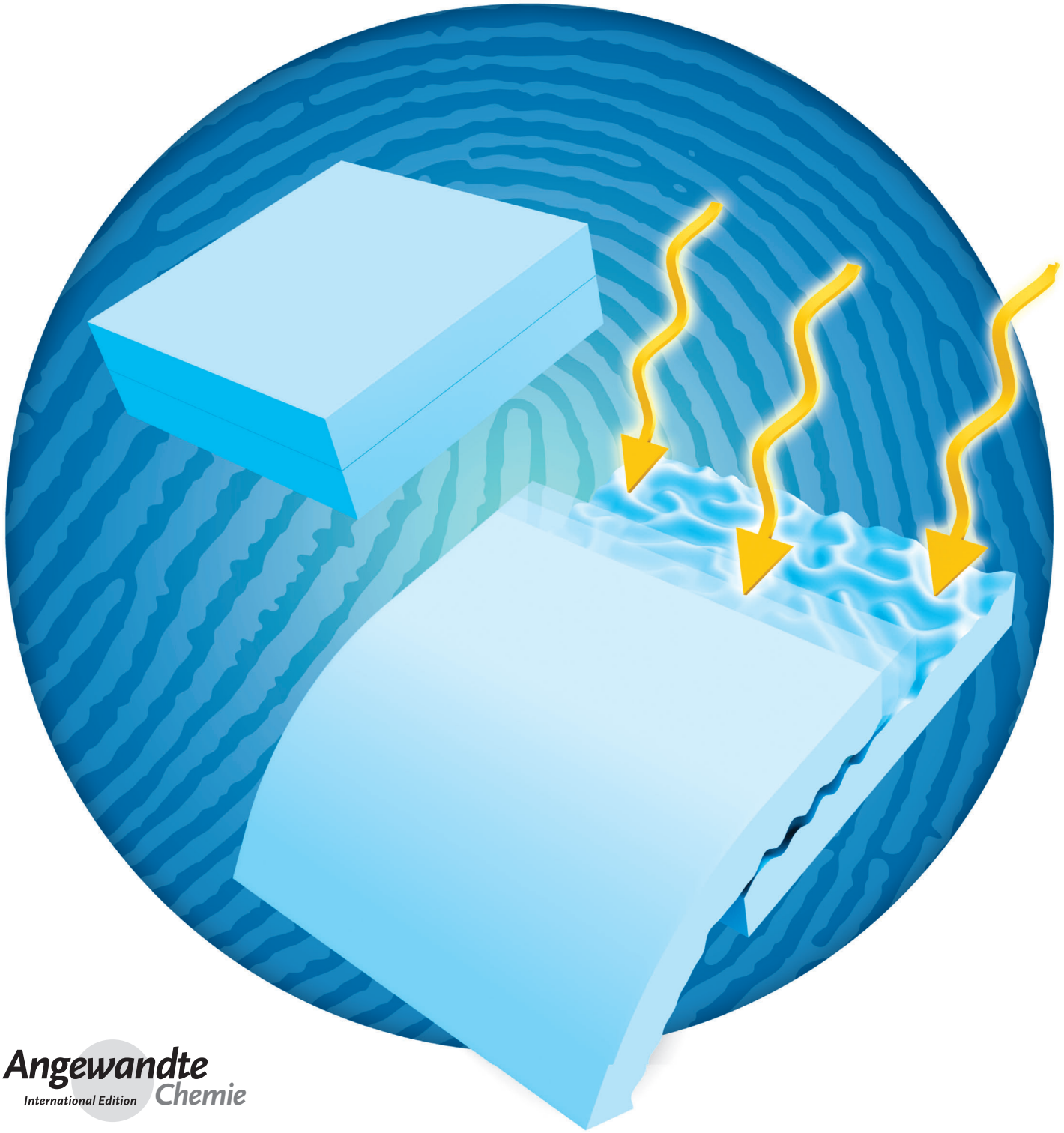

Abstract: *Chiral-nematic polymer network coatings form a "fingerprint" texture through self-assembly. For this purpose the molecular helix of the coating is oriented parallel to the substrate. The coating has a flat surface but when actuated by light in the presence of a copolymerized azobenzene compound, 3D fingerprint structures appear in the coating. The helix forms protrusions at the positions where the molecules are aligned parallel to the surface and withdraws at the positions where the orientation is perpendicular. This process proceeds rapidly and is reversible, that is, the fingerprint-shaped protrusions disappear when the light is switched off. The texture in the on-state resembles that of a human fingerprint and is used to manipulate the gripping friction of a robotic finger. The friction coefficient drops by a factor of four to five when the fingerprint switched on because of reduced surface contacts.*

Surface topographies provide many functionalities in coatings. For example, the optical properties of thin films are largely affected by transformations in surface structure.[1,2] Sub-micron surface patterns alter the wettability by the so-called Lotus effect.[3] And mechanical properties related to friction[4] and adhesion[5] are of interest in robotics and human/machine interfaces.[6] The range of applications would advance further if it was possible to modulate the surface topography. And although many efforts have been devoted to creating surface patterns[3,7] only a few are capable to form and erase the surface reliefs repeatedly.[8] Herein we propose a new concept to create reversibly switching 3D fingerprints. This approach has the advantage that the coating operates in both dry and wet conditions, unlike hydrogel-based coatings.[9] Moreover, they are formed by a self-assembling process without requiring lithographic procedures, in contrast to the structures published previously.[8,10] Intrinsically the self-assembling gives access to lateral structure dimensions down to micrometer sizes or even smaller. The inactivated coating is flat. When activated by light fingerprints textures pop-up in the coating with an in-depth modulation up to 24% related to the film thickness and lateral dimensions down to the micrometer level. Based on the switchable artificial fingerprints we demonstrate a controllable friction for robotic grasping and releasing. These artificial fingerprints resemble those of humans in shape and structure and are potentially suited for integration in robot fingertips. Inactivated fingerprints are flat which offers the maximum contact area with the objects. When addressed with UV light, the 3D fingerprints appear and consequently decrease the contact area which reduces its surface friction and promotes easy release. Grasping is retained through erasing the fingerprints by switching off the UV light.

Liquid-crystal network (LCN) technology has been used for the fabrication of soft actuators.[11] The underlying mechanism is based on the anisotropic deformation caused by changes in the order parameter of the liquid-crystal rod-like moieties embedded in the network. Herein, we present a new technology to fabricate micrometer-sized dynamic corrugations. In their monomeric state liquid-crystal (LC) molecules self-organize by orienting their longitudinal axes along a common director. In chiral Liquid-crystal films the director describes a helix, often with the helix axis normal to the substrate. In this case, we modified the substrate to provide a strong perpendicular anchoring force to the liquid-crystal molecules. Consequently, the orientation of the helix axes is brought parallel to the substrate surface as schematically shown in Figure 1a. In the absence of other directional forces the helix axes form worm-like fingerprint textures, as is shown by the microscope image in Figure 1b (more fingerprint textures are shown in Supporting Information Figure S1).

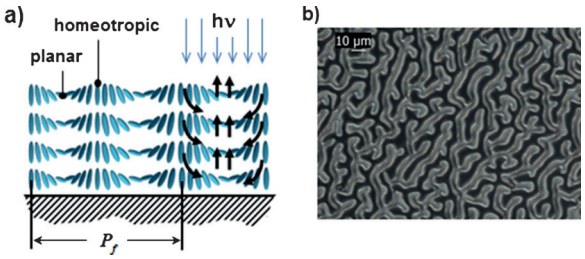

Figure 1. Representation of cholesteric liquid-crystal networks. a) Schematic representation of the dynamics of the fingerprints. b) Polarized optical microscopy images of a fingerprint texture as observed between crossed polarizers. Bright regions correspond to planar and black areas to homeotropic orientation.

We produced liquid-crystal network fingerprints by spin coating the reactive liquid-crystal monomer mixture on a glass plate with a homeotropic polyimide orientation layer. The monomer mixture consists of a homogeneous blend of liquid-crystal mono- and diacrylates, an acrylate chiral dopant, an acrylate azobenzene, and the photoinitiator. Details are given in the Supporting Information (Experimental details, Table S1–S2, Movie S1). The polymerized liquid-crystal network film has an almost flat surface with only a minor relief under 50 nm. Figure 2a shows the initial surface profile measured by confocal microscopy. The initial minor relief is attributed to the Marangoni effect in the monomeric phase which stems from small differences in surface energy between planar and homeotropic orientations.[12] When the film is exposed to UV light the azobenzene undergoes its *trans* to *cis* isomerization and decreases the order parameter of the liquid-crystal network. At the points of planar anchoring, the surface forms protrusions while at the homeotropic positions it forms wells, as shown by confocal microscopy (Figure 2b). These changes result in large height differences randomly

[*] Dr. D. Liu, Dr. D. J. Broer
Laboratory of Functional Organic Materials & Devices (SFD)
Department of Chemical Engineering & Chemistry
Eindhoven University of Technology
Den Dolech 2, 5612 AZ Eindhoven (The Netherlands)
E-mail: d.broer@tue.nl
Dr. D. J. Broer
Institute for Complex Molecular Systems (ICMS)
P.O. Box 513, 5600 MB Eindhoven (The Netherlands)

[**] The results presented are part a research program financed by the Dutch Polymer Institute (DPI), project no 775.

Supporting information for this article is available on the WWW under http://dx.doi.org/10.1002/anie.201400470.

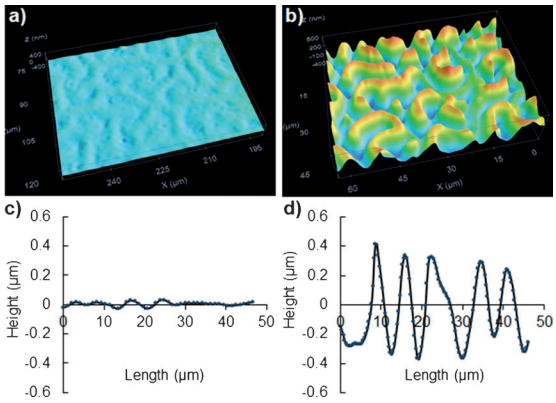

Figure 2. Confocal microscopic images of fingerprints. a) 3D image of the initial flat state and c) Its surface profile. b) 3D image of surface topographies under UV exposure and d) Its surface profile.

distributed over the surface. Relaxation to the flat surface occurs within 60 s. This is much faster than the relaxation times often observed for azobenzene in solution.[13] We attribute this to the mechanochemical stimulation of the *cis*-to-*trans* back reaction of the azobenzene embedded in the liquid-crystal. In this specific example, containing 5 wt. % of azobenzene, the thickness of the coating is 2.5 μm and the height difference of the structures formed is 0.6 μm, which is 24 % of the initial height.

We explain the formation of this significant surface topography by a mechanism where dichroic effects, the order parameter reduction, and the free-volume effect are working together in concert. Because of the dichroic nature of the azobenzene molecules, the parallel aligned molecules have a more dominant absorption of the incoming light. This intensifies the photomechanical effect. From our previous research on standing helices we know that distortion of the order parameter also leads to a density decrease, hence a volume increase, of around 10 %.[10] In the specific fingerprint configuration light that is absorbed in the homeotropic region leads to a transversal expansion in the film plane upon reduction of the order parameter which deforms the planar area even further. Despite the average orientation is homeotropic there is still enough light absorption to address the azobenzene moieties by light incoming along the normal.

To elaborate further on this principle we investigated the relevant parameters such as the pitch of the chiral-nematic helix, the azobenzene concentration, and the UV intensity. Under unconstrained conditions, for instance found when the helix is aligned perpendicular to the surface, the pitch of the helix P_p corresponds to a full 2π molecular rotation. P_p relates linearly to the reciprocal of the concentration of the chiral component. Under the appropriate conditions related to the ratio between thickness d and pitch of the helix P_p, with $0.3 < d/P_p < 0.5$ and supported by strong homeotropic surface anchoring, the planar helix configuration is obtained. We observed that the actual pitch P_f as defined in Figure 1 a, deviates from P_p, a phenomenon which is described in literatures for other chiral liquid crystals.[14] It appeared that the fingerprint pitch P_f relates to P_p as $P_f = i P_p$, depending on the anchoring strength $i = 1$, 2, or 4 (Figure 3 a). For the

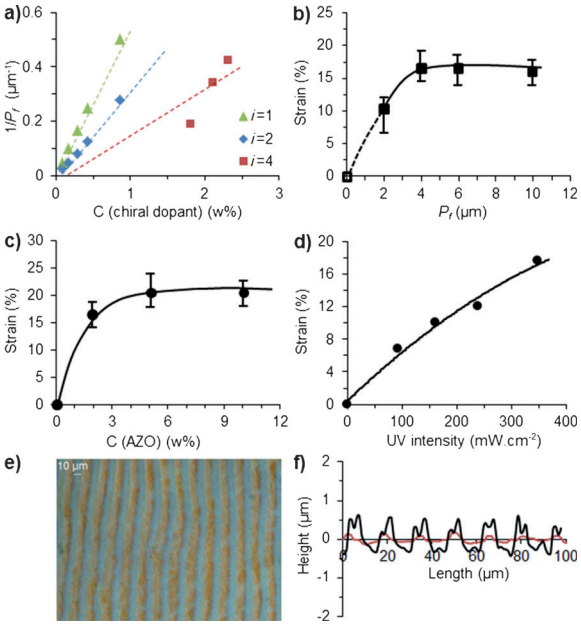

Figure 3. Analysis of the fingerprints. a) Pitch dependence on chiral dopant for different surface anchoring conditions. b) The effect of pitch on the strain of fingerprints, the azobenzene concentration is 2 wt. %. c) The effect of azobenzene (AZO) concentration on the strain of fingerprints. d) The deformation of fingerprints increases with increasing UV intensity. e) The polarization optical microscope image of a regular texture and f) The surface profile at the initial non-actuated state (red line) and actuated (black line).

anchoring-free conditions $P_f = P_p$ and $i = 1$. With increasing anchoring forces i increases stepwise to 2 or 4. In our specific case i is usually equal to 2. In principle P_f can be varied from sub-micron dimensions to infinite. For our experiments displayed in Figure 3 b we chose to vary P_f between 2 μm and 10 μm. It is good to emphasize that the periodicity of the expanding and retracting areas is half of the pitch. Within the measured range of $P_f = 4$–10 μm the measured strain is about constant. The strain is defined in this case as the modulation height of the structures divided by the initial thickness. At $P_f = 2$ μm the effect becomes smaller and assumingly goes to zero when P_f approaches the hypothetical zero.

The influence of the azobenzene concentration was studied while keeping all other parameters constant. In Figure 3 c we plotted the strain versus the azobenzene concentration. It shows that already at 2 wt. % of azobenzene exhibits a large photo-responsive effect. This demonstrates that the cooperative loss of order of the liquid-crystal network is responsible for the dimensional change rather than the photomechanical effect of the azobenzene molecules alone. The height of the artificial fingerprints can be adjusted by UV light intensity, as seen in Figure 3 d (the corresponding 3D confocal microscope images are shown in the Supporting Information Figure S2). This can be attributed to the level of the photo-stationary state of the *trans*-to-*cis* equilibrium which shifts the conversion into higher values with increasing intensity. In this case, we restricted the UV intensity up to a value of 400 mW cm^{-2} to assure that the photo-response dominates over thermal effects. Thermal effects have been

further investigated and reported in the Supporting Information Figure S3.

The texture of the fingerprint are in general random (Figure 1b, Supporting Information Figure S1) but can also be made more regular. In Figure 3e, we demonstrate a texture with a line structures with the periodicity of around 18 μm. The alignment of the line structure is obtained by applying a unidirectional low-pressure buffing of the polyimide alignment film prior to processing of the liquid crystal monomer mixture.

The actuated fingerprints exhibit a height modulation of over 20% with respect to the initial coating thickness. We use the appearance of the elevated structures to tune the friction force. The kinetic friction force (F_f) of the coating is studied with and without fingerprint structure. It is measured by two coatings sliding against each other at a constant speed under a constant normal load F_N. Details of the setup are shown in the Supporting Information Figure S4. Figure 4a shows the linear relationship between F_f and F_N. The kinetic coefficient friction, is defined as $\mu_k = \frac{F_f}{F_N}$.[15] Basically μ_k is the nature of the coating and independent of the loading. The friction coefficient drops from 0.4–0.5 with a flat coating to 0.1 when the fingerprints are "on". The friction traces in Figure 4b are recorded when the fingerprints are cycled between the "on" and "off" states under a constant load of 0.5 N. The left trace in Figure 4b shows the force during the transition from dark to illuminated. The value of μ_k drops from 0.4 when the coatings are flat to 0.1 when the fingerprints are switched "on". The right trace, records the "off" switch from illuminated to dark; μ_k increases to its original high value within seconds. In the presence of the random fingerprints the contact area is decreased. Based on this observation, we demonstrate a gripper that releases its object upon switching 'on' the fingerprints by UV light. In this experiment we clamped a bare glass plate between two surfaces with fingerprint coating at the inactivated flat state. When activating the lamp the gripper releases its load within 3 seconds (Figure 4c–f). A common problem in microrobots is that objects easily stick to soft gripper tips. This releasing mechanism, based on minimizing the friction, provides a solution for this problem. In fact, the integration of our fingerprints coating on robotic finger tips is a nice example of nature inspired technology.

In the case the coating are provided with the random fingerprints the dynamic friction is reduced. Alternatively, when the fingerprints are given a more organized structure, such as the switchable linear protrusions shown in Figure 3e, the protrusions interlock and consequently the friction increases[16] when the fingerprints are switched on. In this case μ_k increases from 0.4–0.5 to 0.6.

In conclusion, we have presented a new approach in designing smart coatings. Three-dimensional fingerprint structures can be induced and modulated by UV light. The morphology providing the artificial fingerprints forms through self-assembling at molecular level in reactive chiral-nematic liquid-crystals. This innovative method creates dynamic surface patterns with in-plane dimensions ranging from tens of nanometer to infinite without involving the conventional lithographic process. The formed fingerprints exhibit a significant increased strain of more than 20%. This means that we can easily create surface topographies with heights of micrometers in thin polymer coatings. Working towards an application we demonstrated that friction can be modulated by light thereby cycling the friction coefficient between 0.1 to 0.4–0.5. Mimicking robotic fingers we built a gripper that releases its load by switching on the fingerprints. In addition to the use of dynamic friction in controlling grip and release, this could lead to versatile applications, such as tracking light in a solar energy system,[17] liquid mixing or flow regulating in microfluidic channels,[18] and cell growth in biomedical applications.[19]

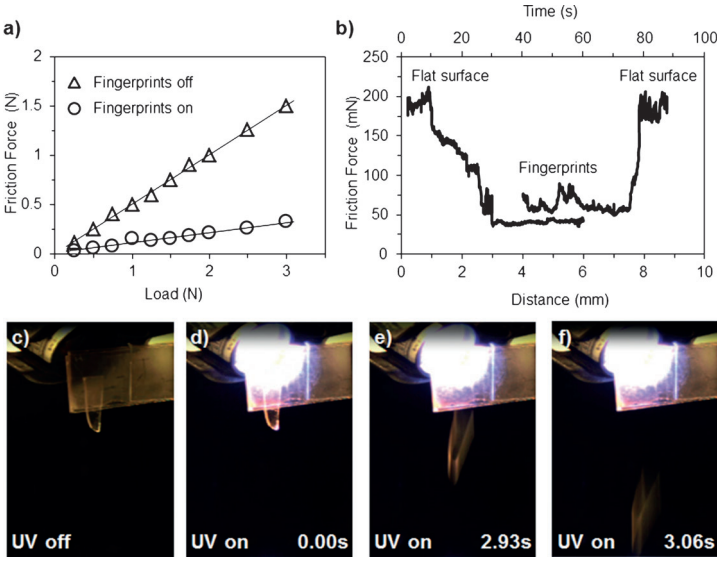

Figure 4. Change of friction between fingerprints "on" and "off". a) Friction forces versus loading and their linear fits. b) Dynamic force traces when switching the fingerprints between "on" and "off". For reasons of clarity the right trace is shifted 10 mN upwards. c)–f) Snapshots of a gripper that releases an object upon UV illumination. The movie is given in the Supporting Information, Movie S2.

Received: January 13, 2014
Published online: March 11, 2014

Keywords: dynamic surfaces · fingerprints · friction · liquid crystals · photochemistry

[1] C. J. Ting, C. F. Chen, C. P. Chou, *Opt. Commun.* **2009**, *282*, 434–438.
[2] L. Dong, A. K. Agarwal, D. J. Beebe, H. Jiang, *Nature* **2006**, *442*, 551–554.
[3] a) J. Y. Chung, J. P. Youngblood, C. M. Stafford, *Soft Matter* **2007**, *3*, 1163–1169; b) Z.-Z. Gu, H. Uetsuka, K. Takahashi, R. Nakajima, H. Onishi, A. Fujishima, O. Sato, *Angew. Chem.* **2003**, *115*, 922–925; *Angew. Chem. Int. Ed.* **2003**, *42*, 894–897.
[4] M. Varenberg, S. N. Gorb, *Adv. Mater.* **2009**, *21*, 483–486.
[5] M. D. Bartlett, A. B. Croll, A. J. Crosby, *Adv. Funct. Mater.* **2012**, *22*, 4985–4992.
[6] Y. Bar-Cohen, *IJASS* **2012**, *13*, 1–13.

[7] a) Y. Gritsai, L. M. Goldenberg, J. Stumpe, *Opt. Express* **2011**, *19*, 18687 – 18695; b) H. E. Jeong, M. K. Kwak, K. Y. Suh, *Langmuir* **2010**, *26*, 2223 – 2226; c) M. Guvendiren, S. Yang, J. A. Burdick, *Adv. Funct. Mater.* **2009**, *19*, 3038 – 3045; d) D. P. Holmes, A. J. Crosby, *Adv. Mater.* **2007**, *19*, 3589 – 3593; e) D. M. Drotlef, P. Blümler, A. del Campo, *Adv. Mater.* **2014**, *26*, 775 – 779; f) S. Reddy, E. Arzt, A. del Campo, *Adv. Mater.* **2007**, *19*, 3833 – 3837.

[8] a) D. Liu, C. M. W. Bastiaansen, J. M. J. den Toonder, D. J. Broer, *Angew. Chem.* **2012**, *124*, 916 – 920; *Angew. Chem. Int. Ed.* **2012**, *51*, 892 – 896; b) J. Yoon, P. Bian, J. Kim, T. J. McCarthy, R. C. Hayward, *Angew. Chem.* **2012**, *124*, 7258 – 7261; *Angew. Chem. Int. Ed.* **2012**, *51*, 7146 – 7149; c) M. E. Sousa, D. J. Broer, C. W. M. Bastiaansen, L. B. Freund, G. P. Crawford, *Adv. Mater.* **2006**, *18*, 1842 – 1845.

[9] D. Liu, C. W. M. Bastiaansen, J. M. J. Toonder, D. J. Broer, *Langmuir* **2013**, *29*, 5622 – 5629.

[10] D. Liu, C. M. W. Bastiaansen, J. M. J. den Toonder, D. J. Broer, *Macromolecules* **2012**, *45*, 8005 – 8012.

[11] a) J. S. Evans, P. J. Ackerman, D. J. Broer, J. Lagemaat, I. I. Smalyukh, *Phys. Rev. E* **2013**, *87*, 032503; b) M. Warner, C. D. Modes, D. Corbett, *Proc. R. Soc. London Ser. A* **2010**, *466*, 2975 – 2989; c) M. Camacho-Lopez, H. Finkelmann, P. Palffy-Muhoray, M. Shelley, *Nat. Mater.* **2004**, *3*, 307 – 310; d) T. J. White, S. V. Serak, N. V. Tabiryan, R. A. Vaia, T. J. Bunning, *J. Mater. Chem.* **2009**, *19*, 1080 – 1085; e) C. L. Van Oosten, C. W. M. Bastiaansen, D. J. Broer, *Nat. Mater.* **2009**, *8*, 677 – 682; f) T. Kosa, L. Sukhomlinova, L. Su, B. Taheri, T. J. White, T. J. Bunning, *Nature* **2012**, *485*, 347 – 349; g) Y. Yu, M. Nakano, T. Ikeda, *Nature* **2003**, *425*, 145 – 145; h) J. Cui, D. M. Drotlef, I. Larraza, J. P. Fernández-Blázquez, L. F. Boesel, C. Ohm, M. Mezger, R. Zentel, A. del Campo, *Adv. Mater.* **2012**, *24*, 4601 – 4604.

[12] R. Eelkema, M. M. Pollard, J. Vicario, V. Katsonis, B. S. Ramon, C. W. M. Bastiaansen, D. J. Broer, B. L. Feringa, *Nature* **2006**, *440*, 163 – 163.

[13] A. A. Beharry, G. A. Woolley, *Chem. Soc. Rev.* **2011**, *40*, 4422 – 4437.

[14] a) T. Frisch, L. Gil, J. M. Gilli, *Phys. Rev. E* **1993**, *48*, R4199 – R4202; b) J. Baudry, M. Brazovskaia, L. Lejcek, P. Oswald, S. Pirkl, *Liq. Cryst.* **1996**, *21*, 893 – 901.

[15] R. P. Kusv, J. Q. Whitley, *J. Biomech.* **1990**, *23*, 913 – 925.

[16] C. Pang, T. Kim, W. G. Bae, D. Kang, S. M. Kim, K.-Y. Suh, *Adv. Mater.* **2012**, *24*, 475 – 479.

[17] M. Ibn-Elhaj, M. Schadt, *Nature* **2001**, *410*, 796 – 799.

[18] A. D. Stroock, S. K. W. Dertinger, A. Ajdari, I. Mezić, H. A. Stone, G. M. Whitesides, *Science* **2002**, *295*, 647 – 651.

[19] V. Jayawarna, *Adv. Mater.* **2006**, *18*, 611 – 614.

